Receding Horizon Trajectory Optimization in Opportunistic Navigation Environments

Zaher M. Kassas, *Senior Member, IEEE*, and Todd E. Humphreys, *Member, IEEE*

***Abstract*—Receding horizon trajectory optimization for optimal information gathering in opportunistic navigation environments is considered. A receiver is assumed to be dropped in an environment comprising multiple signals of opportunity (SOPs) transmitters. The receiver has minimal *a priori* knowledge about its own states and the SOPs' states. The receiver draws pseudorange observations from the SOPs. The receiver's objective is to build a high-fidelity signal landscape map while simultaneously localizing itself within this map in space and time. Assuming that the receiver can control its maneuvers, the following two problems are considered. First, the minimal conditions under which the environment is completely observable are established. It is shown that receiver-controlled maneuvers reduce the minimal *a priori* information about the environment required for complete observability. Second, the trajectories that the receiver should traverse are prescribed. To this end, a one-step look-ahead (greedy) strategy is compared with a multi-step look-ahead (receding horizon) strategy. The limitations and achieved improvements in the map quality and space-time localization accuracy due to the receding horizon strategy are quantified. The computational burden associated with the receding horizon strategy is also discussed.**

***Index Terms*—Trajectory optimization, receding horizon, adaptive sensing, motion planning, radionavigation, signals of opportunity, opportunistic navigation**

I. Introduction

Opportunistic navigation (OpNav) aims to extract position and timing information from ambient radio signals of opportunity (SOPs) to improve navigation robustness in Global Navigation Satellite System (GNSS)-challenged environments [1]. OpNav treats all signals as potential SOPs, from conventional GNSS signals to communications signals never intended for use as timing or positioning sources, such as signals from cellular towers [2], digital video broadcasting [3], Iridium satellites [4], and ultrawideband orthogonal frequency division multiplexed radar [5]. In collaborative OpNav (COpNav), multiple OpNav receivers share information to construct and continuously refine a global signal landscape [6].

The OpNav estimation problem is similar to the simultaneous localization and mapping (SLAM) problem in robotics [7], [8]. Both imagine an agent which, starting with incomplete knowledge of its location and surroundings, simultaneously builds a map of its environment and locates itself within that map. In traditional SLAM, as the robot moves through the environment, it constructs a map that is composed of landmarks with associated positions. OpNav extends this concept to radio signals, with SOPs playing the role of landmarks. In contrast to a SLAM environmental map, the OpNav signal landscape is dynamic and more complex. In pseudorange-only OpNav, the receiver must simultaneously estimate its own states and the states of each SOP. The latter comprise, for each transmitter, the position and velocity, the time offset from a reference time base, the rate of change of time offset, and optionally a set of parameters that characterize the stability of the transmitter's oscillator. The signal landscape map can be thought of metaphorically as a "jello map," with the jello firmer as the oscillators become more stable.

A receiver entering a new signal landscape may have minimal *a priori* knowledge about its own states and the SOPs' states. The observability of planar COpNav environments comprising multiple receivers with velocity random walk dynamics making pseudorange measurements on multiple SOPs was thoroughly analyzed in [9], [10], and the degree of observability, also known as estimability, of the various states was quantified in [11]. Observability is a Boolean property: it asserts whether a system is observable or not. It does not specify which trajectory is best for information gathering and, consequently, estimability. Such trajectory optimization is the subject of this paper. Accordingly, the receiver dynamics are modified to permit receiver-controlled maneuvers.

In tracking problems, optimizing the observer's path has been studied extensively [12]–[14]. In such problems, the observer, which is assumed to have perfect knowledge of its own states, tracks a mobile target. The trajectory optimization objective is to prescribe trajectories for the observer to maintain good estimates of the target's states. In SLAM, the problem of trajectory optimization is more involved due to the coupling between the localization accuracy and map quality [15]–[17].

In OpNav environments, trajectory optimization can be thought of as a hybrid of (i) optimizing an observer's path in tracking problems and (ii) optimizing the robot's path in SLAM. First, due to the dynamical nature of the clock error states, the SOP's state space is non-stationary, which makes the problem analogous to tracking non-stationary targets. Second, the similarity to SLAM stems from the coupling between the receiver space-time localization accuracy and signal landscape fidelity. A particular feature of OpNav is that the quality of the estimates not only depends on the spatial trajectory the receiver traverses within the environment, but also on the velocity with which the receiver traverses such trajectory [18].

Receiver trajectory optimization in OpNav environments

Z.M. Kassas is with the Department of Electrical Engineering, The University of California, Riverside. Address: Suite 343 Winston Chung Hall, Riverside, CA 92521, USA (email: zkassas@ieee.org).

T.E. Humphreys is with the Department of Aerospace Engineering and Engineering Mechanics, The University of Texas at Austin. Address: W.R. Woolrich Laboratories, C0600, 210 East 24th Street, Austin, TX 78712, USA (email: todd.humphreys@mail.utexas.edu).

was initially studied in [18], where the following problem was considered. A receiver with no *a priori* knowledge about its own states is dropped in an OpNav environment comprising multiple SOPs. Assuming that the receiver could prescribe its own trajectory in the form of velocity commands, what motion planning strategy should the receiver adopt to build a high-fidelity map of the OpNav signal landscape, while simultaneously localizing itself within this map in space and time? To address this question, an optimal closed-loop information-theoretic one-step look-ahead, also known as greedy, strategy was proposed for receiver motion planning. Three information measures were compared: D-optimality, A-optimality, and E-optimality [19]. It was demonstrated that greedy strategies outperformed a receiver moving randomly or in a pre-defined trajectory. Among these measures, D-optimality yielded less estimation error than A-optimality and E-optimality criteria. Active collaborative signal landscape map building was addressed in [20], where four decision making and information fusion architectures were studied: decentralized, centralized, and hierarchical with and without feedback. It was demonstrated that the hierarchical with feedback architecture achieves a negligible price of anarchy (PoA). The PoA measures the degradation in the solution quality should the receivers produce their own maps and make their own maneuver decisions versus a completely centralized approach.

Multi-step look-ahead, also known as receding horizon, strategies are known to outperform greedy strategies for trajectory optimization [16], [21], [22]. An initial study of receding horizon receiver trajectory optimization in OpNav environments was conducted in [23]; however, only the problem of simultaneous receiver localization and signal landscape mapping was tackled, only single-run simulation results were presented, and the observability conclusions were offered without proofs. This paper's contribution is to extend [23] in two ways. First, it presents rigorous nonlinear observability-based proofs showing that receiver-controlled maneuvers reduce the *a priori* knowledge required about the COpNav environment for complete observability. Second, it studies the achieved improvements and associated limitations of a receding horizon strategy over a greedy strategy for the two observable modes of operation: (i) simultaneous receiver localization and signal landscape mapping and (ii) signal landscape mapping. Single-run and Monte Carlo (MC) based simulations are presented to conclude that receding horizon trajectory optimization is more effective in the signal landscape mapping mode. Moreover, it is demonstrated that the advantages of receding horizon diminish as the system uncertainty in the form of observation noise increases. For the sake of simplicity, this paper considers planar environments. Extensions to three-dimensions is anticipated to be straightforward.

The remainder of this paper is organized as follows. Section II describes the COpNav environment dynamics and observation models. Section III analyzes COpNav observability. Section IV formulates the receding horizon receiver trajectory optimization problem and discusses the associated computational burden. Section V presents simulation results comparing the achieved signal landscape map quality and space-time localization accuracy from random, greedy, and receding horizon trajectories. Concluding remarks are given in Section VI.

II. Model Description

A. Dynamics Model

The receiver's dynamics will be assumed to evolve according to the controlled velocity random walk model. An object moving according to such dynamics in a generic coordinate ξ has the dynamics

$$\ddot{\xi}(t) = u(t) + \tilde{w}_\xi(t),$$

where $u(t)$ is the control input in the form of an acceleration command and $\tilde{w}_\xi(t)$ is a zero-mean white noise process with power spectral density $\tilde{q}_\xi$, i.e.,

$$\mathbb{E}\left[\tilde{w}_\xi(t)\right] = 0, \quad \mathbb{E}\left[\tilde{w}_\xi(t)\tilde{w}_\xi(\tau)\right] = \tilde{q}_\xi\,\delta(t-\tau),$$

where $\delta(t)$ is the Dirac delta function. The receiver and SOP clock error dynamics will be modeled according to the two-state model composed of the clock bias δt and clock drift $\dot{\delta t}$. The clock error states evolve according to

$$\dot{\boldsymbol{x}}_{\rm clk}(t) = \mathbf{A}_{\rm clk}\,\boldsymbol{x}_{\rm clk}(t) + \tilde{\boldsymbol{w}}_{\rm clk}(t),$$

$$\boldsymbol{x}_{\rm clk} = \begin{bmatrix} \delta t \\ \dot{\delta t} \end{bmatrix}, \quad \tilde{\boldsymbol{w}}_{\rm clk} = \begin{bmatrix} \tilde{w}_{\delta t} \\ \tilde{w}_{\dot{\delta t}} \end{bmatrix}, \quad \mathbf{A}_{\rm clk} = \begin{bmatrix} 0 & 1 \\ 0 & 0 \end{bmatrix},$$

where $\tilde{w}_{\delta t}$ and $\tilde{w}_{\dot{\delta t}}$ are modeled as zero-mean, mutually independent white noise processes with power spectra $S_{\tilde{w}_{\delta t}}$ and $S_{\tilde{w}_{\dot{\delta t}}}$, respectively. The power spectra $S_{\tilde{w}_{\delta t}}$ and $S_{\tilde{w}_{\dot{\delta t}}}$ can be related to the power-law coefficients $\{h_\alpha\}_{\alpha=-2}^{2}$, which have been shown through laboratory experiments to be adequate to characterize the power spectral density of the fractional frequency deviation $y(t)$ of an oscillator from nominal frequency, which takes the form $S_y(f) = \sum_{\alpha=-2}^{2} h_\alpha f^\alpha$ [24]. It is common to approximate the clock error dynamics by considering only the frequency random walk coefficient h_{-2} and the white frequency coefficient h_0, which lead to $S_{\tilde{w}_{\delta t}} \approx \frac{h_0}{2}$ and $S_{\tilde{w}_{\dot{\delta t}}} \approx 2\pi^2 h_{-2}$ [25].

The receiver's state vector will be defined by augmenting the receiver's planar position $\boldsymbol{r}_r$ and velocity $\dot{\boldsymbol{r}}_r$ with its clock error states $\boldsymbol{x}_{\rm clk}$ to yield the state space realization

$$\dot{\boldsymbol{x}}_r(t) = \mathbf{A}_r\,\boldsymbol{x}_r(t) + \mathbf{B}_r\,\boldsymbol{u}_r(t) + \mathbf{D}_r\,\tilde{\boldsymbol{w}}_r(t), \tag{1}$$

where $\boldsymbol{x}_r = \left[\boldsymbol{r}_r^{\mathsf{T}},\, \dot{\boldsymbol{r}}_r^{\mathsf{T}},\, \delta t_r,\, \dot{\delta t}_r\right]^{\mathsf{T}}$, $\boldsymbol{r}_r = \left[x_r,\, y_r\right]^{\mathsf{T}}$, $\boldsymbol{u}_r = \left[u_x,\, u_y\right]^{\mathsf{T}}$, $\tilde{\boldsymbol{w}}_r = \left[\tilde{w}_x,\, \tilde{w}_y,\, \tilde{w}_{\delta t_r},\, \tilde{w}_{\dot{\delta t}_r}\right]^{\mathsf{T}}$,

$$\mathbf{A}_r = \begin{bmatrix} \mathbf{0}_{2\times2} & \mathbf{I}_{2\times2} & \mathbf{0}_{2\times2} \\ \mathbf{0}_{2\times2} & \mathbf{0}_{2\times2} & \mathbf{0}_{2\times2} \\ \mathbf{0}_{2\times2} & \mathbf{0}_{2\times2} & \mathbf{A}_{\rm clk} \end{bmatrix}, \; \mathbf{B}_r = \begin{bmatrix} \mathbf{0}_{2\times2} \\ \mathbf{I}_{2\times2} \\ \mathbf{0}_{2\times2} \end{bmatrix}, \; \mathbf{D}_r = \begin{bmatrix} \mathbf{0}_{2\times4} \\ \mathbf{I}_{4\times4} \end{bmatrix}.$$

The receiver's dynamics in (1) is discretized at a constant sampling period $T \triangleq t_{k+1} - t_k$, assuming zero-order hold of the control inputs, i.e., $\{u(t) = u(t_k),\, t_k \le t < t_{k+1}\}$, to yield the discrete-time (DT) model

$$\boldsymbol{x}_r\left(t_{k+1}\right) = \mathbf{F}_r\,\boldsymbol{x}_r(t_k) + \mathbf{G}_r\,\boldsymbol{u}_r(t_k) + \boldsymbol{w}_r(t_k), \;\; k = 0, 1, 2, \ldots$$

where $\boldsymbol{w}_r$ is a DT zero-mean white noise sequence with covariance $\mathbf{Q}_r = \mathrm{diag}\left[\mathbf{Q}_{\mathrm{pv}},\, \mathbf{Q}_{\mathrm{clk},r}\right]$, where

$$\mathbf{F}_r = \begin{bmatrix} \mathbf{I}_{2\times2} & T\mathbf{I}_{2\times2} & \mathbf{0}_{2\times2} \\ \mathbf{0}_{2\times2} & \mathbf{I}_{2\times2} & \mathbf{0}_{2\times2} \\ \mathbf{0}_{2\times2} & \mathbf{0}_{2\times2} & \mathbf{F}_{\mathrm{clk}} \end{bmatrix},\ \mathbf{G}_r = \begin{bmatrix} \frac{T^2}{2}\mathbf{I}_{2\times2} \\ T\,\mathbf{I}_{2\times2} \\ \mathbf{0}_{2\times2} \end{bmatrix},\ \mathbf{F}_{\mathrm{clk}} = \begin{bmatrix} 1 & T \\ 0 & 1 \end{bmatrix}$$

$$\mathbf{Q}_{\mathrm{clk},r} = \begin{bmatrix} S_{\tilde{w}_{\delta t_r}} T + S_{\tilde{w}_{\dot{\delta} t_r}} \frac{T^3}{3} & S_{\tilde{w}_{\dot{\delta} t_r}} \frac{T^2}{2} \\ S_{\tilde{w}_{\dot{\delta} t_r}} \frac{T^2}{2} & S_{\tilde{w}_{\dot{\delta} t_r}} T \end{bmatrix}$$

$$\mathbf{Q}_{\mathrm{pv}} = \begin{bmatrix} \tilde{q}_x \frac{T^3}{3} & 0 & \tilde{q}_x \frac{T^2}{2} & 0 \\ 0 & \tilde{q}_y \frac{T^3}{3} & 0 & \tilde{q}_y \frac{T^2}{2} \\ \tilde{q}_x \frac{T^2}{2} & 0 & \tilde{q}_x T & 0 \\ 0 & \tilde{q}_y \frac{T^2}{2} & 0 & \tilde{q}_y T \end{bmatrix}.$$

The SOP will be assumed to emanate from a spatially-stationary terrestrial transmitter whose state consists of its planar position and clock error states. Hence, the SOP's dynamics can be described by the state space model

$$\dot{\boldsymbol{x}}_s(t) = \mathbf{A}_s\, \boldsymbol{x}_s(t) + \mathbf{D}_s \tilde{\boldsymbol{w}}_s(t), \tag{2}$$

where $\boldsymbol{x}_s = \left[\boldsymbol{r}_s^{\mathsf{T}},\, \delta t_s,\, \dot{\delta t}_s\right]^{\mathsf{T}}$, $\boldsymbol{r}_s = [x_s,\, y_s]^{\mathsf{T}}$, $\tilde{\boldsymbol{w}}_s = \left[\tilde{w}_{\delta t_s},\, \tilde{w}_{\dot{\delta} t_s}\right]^{\mathsf{T}}$

$$\mathbf{A}_s = \begin{bmatrix} \mathbf{0}_{2\times2} & \mathbf{0}_{2\times2} \\ \mathbf{0}_{2\times2} & \mathbf{A}_{\mathrm{clk}} \end{bmatrix}, \quad \mathbf{D}_s = \begin{bmatrix} \mathbf{0}_{2\times2} \\ \mathbf{I}_{2\times2} \end{bmatrix}.$$

Discretizing the SOP's dynamics (2) at a sampling interval T yields the DT-equivalent model

$$\boldsymbol{x}_s\left(t_{k+1}\right) = \mathbf{F}_s\, \boldsymbol{x}_s(t_k) + \boldsymbol{w}_s(t_k),$$

where $\boldsymbol{w}_s$ is a DT zero-mean white noise sequence with covariance $\mathbf{Q}_s$, and

$$\mathbf{F}_s = \mathrm{diag}\left[\mathbf{I}_{2\times2},\, \mathbf{F}_{\mathrm{clk}}\right], \quad \mathbf{Q}_s = \mathrm{diag}\left[\mathbf{0}_{2\times2},\, \mathbf{Q}_{\mathrm{clk},s}\right],$$

where $\mathbf{Q}_{\mathrm{clk},s}$ is identical to $\mathbf{Q}_{\mathrm{clk},r}$, except that $S_{\tilde{w}_{\delta t_r}}$ and $S_{\tilde{w}_{\dot{\delta} t_r}}$ are now replaced with SOP-specific spectra, $S_{\tilde{w}_{\delta t_s}}$ and $S_{\tilde{w}_{\dot{\delta} t_s}}$, respectively.

Defining the augmented state vector $\boldsymbol{x} \triangleq \left[\boldsymbol{x}_r^{\mathsf{T}},\, \boldsymbol{x}_s^{\mathsf{T}}\right]^{\mathsf{T}}$, the augmented process noise vector $\boldsymbol{w} \triangleq \left[\boldsymbol{w}_r^{\mathsf{T}},\, \boldsymbol{w}_s^{\mathsf{T}}\right]^{\mathsf{T}}$, and $\boldsymbol{u} \triangleq \boldsymbol{u}_r$, yields the system dynamics

$$\boldsymbol{x}\left(t_{k+1}\right) = \mathbf{F}\, \boldsymbol{x}\left(t_k\right) + \mathbf{G}\, \boldsymbol{u}\left(t_k\right) + \boldsymbol{w}(t_k), \tag{3}$$

where $\mathbf{F} = \mathrm{diag}\left[\mathbf{F}_r,\, \mathbf{F}_s\right]$, $\mathbf{G} = \left[\mathbf{G}_r^{\mathsf{T}}, \mathbf{0}_{4\times2}^{\mathsf{T}}\right]^{\mathsf{T}}$, and $\boldsymbol{w}$ is a zero-mean white noise sequence with covariance $\mathbf{Q} = \mathrm{diag}\left[\mathbf{Q}_r, \mathbf{Q}_s\right]$. While the model defined in (3) considers only one receiver and one SOP, it can be readily extended to multiple receivers and multiple SOPs by further augmentation.

B. Observation Model

To properly model the pseudorange observations, one must consider three different time systems. The first is true time, denoted by the variable t, which can be considered equivalent to Global Positioning System (GPS) time. The second time system is that of the receiver's clock and is denoted t_r. The third time system is that of the SOP's clock and is denoted t_s. The three time systems are related to each other according to

$$t = t_r - \delta t_r(t), \qquad t = t_s - \delta t_s(t),$$

where $\delta t_r(t)$ and $\delta t_s(t)$ are the amounts by which the receiver and SOP clocks are different from true time, respectively.

The pseudorange observation made by the receiver on an SOP is made in the receiver time and is modeled according to

$$\begin{aligned} \rho(t_r) = {} & \\ & \left\|\boldsymbol{r}_r\left[t_r - \delta t_r(t_r)\right] - \boldsymbol{r}_s\left[t_r - \delta t_r(t_r) - \delta t_{\mathrm{TOF}}\right]\right\|_2 + \\ & c\,.\left\{\delta t_r(t_r) - \delta t_s\left[t_r - \delta t_r(t_r) - \delta t_{\mathrm{TOF}}\right]\right\} + \tilde{v}_\rho(t_r), \end{aligned} \tag{4}$$

where c is the speed of light, δt_{TOF} is the time-of-flight of the signal from the SOP to the receiver, and $\tilde{v}_\rho$ is the error in the pseudorange measurement, which is modeled as a zero-mean white Gaussian noise process with power spectral density $\tilde{r}$ [26]. The clock offsets δt_r and δt_s in (4) were assumed to be small and slowly changing, in which case $\delta t_r(t) = \delta t_r\left[t_r - \delta t_r(t)\right] \approx \delta t_r(t_r)$. The first term in (4) is the true range between the receiver's position at time of reception and the SOP's position at time of transmission of the signal, while the second term arises due to the offsets from true time in the receiver and SOP clocks.

The observation model in (4) can be further simplified by converting it to true time and invoking mild approximations, discussed in [10], to arrive at

$$\begin{aligned} z(t) = \rho(t) \triangleq {} & y(t) + \tilde{v}_\rho(t) \\ \approx {} & \left\|\boldsymbol{r}_r(t) - \boldsymbol{r}_s(t)\right\|_2 + c \cdot \left[\delta t_r(t) - \delta t_s(t)\right] + \tilde{v}_\rho(t), \end{aligned} \tag{5}$$

where y is the noise-free observation. Discretizing the observation equation (5) at a sampling interval T yields the DT-equivalent model

$$\begin{aligned} z(t_k) = {} & y(t_k) + v_\rho(t_k) \\ = {} & \left\|\boldsymbol{r}_r(t_k) - \boldsymbol{r}_s(t_k)\right\|_2 + c \cdot \left[\delta t_r(t_k) - \delta t_s(t_k)\right] + v_\rho(t_k), \end{aligned} \tag{6}$$

where v_ρ is a DT zero-mean white Gaussian sequence with variance $r = \tilde{r}/T$.

III. Observability Analysis

The observability of COpNav environments comprising multiple receivers with velocity random walk dynamics, i.e., without controlled maneuvers, making pseudorange observations on multiple SOPs, was considered in [10] via linear observability tools. The objective of that observability analysis was twofold: (i) determine the minimal required *a priori* knowledge about the environment for full observability, and (ii) in cases where the environment is not fully observable, determine the observable states, if any. In this section, the COpNav observability analysis is extended to study the effects of allowing the receivers to actively control their maneuvers. To this end, and in contrast with the linear observability tools invoked in [10], the observability is analyzed here via nonlinear observability tools. As will be shown, the observability conditions with control are less stringent than those without control.

A. Observability of Nonlinear Systems

For nonlinear systems, it is more appropriate to analyze observability through nonlinear observability tools rather than

by linearizing the nonlinear system and applying linear observability tools, for two reasons: (i) nonlinear observability tools capture the nonlinearities of the dynamics and observations, and (ii) while the control inputs are never considered in the linear observability tools, they are explicitly taken into account in the nonlinear observability tools [27].

For the sake of clarity and self-containment, the nonlinear observability test employed in this paper is outlined next. Consider a continuous-time nonlinear dynamic system in the control affine form [28]

$$\Sigma_{\mathrm{NL}}: \begin{cases} \dot{\boldsymbol{x}}(t) = \boldsymbol{f}_0\left[\boldsymbol{x}(t)\right] + \sum_{i=1}^{r} \boldsymbol{f}_i\left[\boldsymbol{x}(t)\right] u_i, \ \boldsymbol{x}(t_0) = \boldsymbol{x}_0 \\ \boldsymbol{y}(t) = \boldsymbol{h}\left[\boldsymbol{x}(t)\right], \end{cases} \tag{7}$$

where $\boldsymbol{x} \in \mathbb{R}^n$ is the system state vector, $\boldsymbol{u} \in \mathbb{R}^r$ is the control input vector, $\boldsymbol{y} \in \mathbb{R}^m$ is the observation vector, and $\boldsymbol{x}_0$ is an arbitrary initial condition.

Several notions of nonlinear observability exist for Σ_{NL}, namely (global) nonlinear observability, local observability, weak observability, and local weak observability [27]. An algebraic test exists to assess local weak observability, which intuitively means that $\boldsymbol{x}_0$ is instantaneously distinguishable from its neighbors. This test is based on constructing the so-called nonlinear observability matrix defined next.

Definition III.1. *The first-order Lie derivative of a scalar function h with respect to a vector-valued function $\boldsymbol{f}$ is*

$$\mathfrak{L}^1_{\boldsymbol{f}} h(\boldsymbol{x}) \triangleq \sum_{j=1}^{n} \frac{\partial h(\boldsymbol{x})}{\partial x_j} f_j(\boldsymbol{x}) = \left\langle \nabla_{\boldsymbol{x}} h(\boldsymbol{x}), \boldsymbol{f}(\boldsymbol{x}) \right\rangle, \tag{8}$$

where $\boldsymbol{f}(\boldsymbol{x}) \triangleq [f_1(\boldsymbol{x}), \ldots, f_n(\boldsymbol{x})]^{\mathsf{T}}$. The zeroth-order Lie derivative of any function is the function itself, i.e., $\mathfrak{L}^0_{\boldsymbol{f}} h(\boldsymbol{x}) = h(\boldsymbol{x})$. The second-order Lie derivative can be computed recursively as

$$\mathfrak{L}^2_{\boldsymbol{f}} h(\boldsymbol{x}) = \mathfrak{L}_{\boldsymbol{f}} \left[\mathfrak{L}^1_{\boldsymbol{f}} h(\boldsymbol{x})\right] = \left\langle \left[\nabla_{\boldsymbol{x}} \mathfrak{L}^1_{\boldsymbol{f}} h(\boldsymbol{x})\right], \boldsymbol{f}(\boldsymbol{x}) \right\rangle. \tag{9}$$

Higher-order Lie derivatives can be computed similarly. Mixed-order Lie derivatives of $h(\boldsymbol{x})$ with respect to different functions $\boldsymbol{f}_i$ and $\boldsymbol{f}_j$, given the derivative with respect to $\boldsymbol{f}_i$, can be defined as

$$\mathfrak{L}^2_{\boldsymbol{f}_i \boldsymbol{f}_j} h(\boldsymbol{x}) \triangleq \mathfrak{L}^1_{\boldsymbol{f}_j} \left[\mathfrak{L}^1_{\boldsymbol{f}_i} h(\boldsymbol{x})\right] = \left\langle \left[\nabla_{\boldsymbol{x}} \mathfrak{L}^1_{\boldsymbol{f}_i} h(\boldsymbol{x})\right], \boldsymbol{f}_j(\boldsymbol{x}) \right\rangle.$$

The nonlinear observability matrix, denoted $\boldsymbol{\mathcal{O}}_{\mathrm{NL}}$, of Σ_{NL} defined in (7) is a matrix whose rows are the gradients of Lie derivatives, specifically

$$\boldsymbol{\mathcal{O}}_{\mathrm{NL}} \triangleq \left\{ \nabla^{\mathsf{T}}_{\boldsymbol{x}} \left[\mathfrak{L}^p_{\boldsymbol{f}_i, \ldots, \boldsymbol{f}_j} h_l(\boldsymbol{x})\right] \middle| i, j = 0, \ldots, p; \, p = 0, \ldots, n-1; l = 1, \ldots, m \right\} \tag{10}$$

where $\boldsymbol{h}(\boldsymbol{x}) \triangleq [h_1(\boldsymbol{x}), \ldots, h_m(\boldsymbol{x})]^{\mathsf{T}}$.

The significance of $\boldsymbol{\mathcal{O}}_{\mathrm{NL}}$ is that it can be employed to furnish necessary and sufficient conditions for local weak observability [27], [29]. In particular, if $\boldsymbol{\mathcal{O}}_{\mathrm{NL}}$ is full-rank, then Σ_{NL} is said to satisfy the observability rank condition, in which case the system is locally weakly observable. Moreover, if a system Σ_{NL} is locally weakly observable, then the observability rank condition is satisfied generically. The term "generically" means that $\boldsymbol{\mathcal{O}}_{\mathrm{NL}}$ is full-rank everywhere, except possibly within a subset of the domain of $\boldsymbol{x}$ [30].

B. Scenarios Overview

The various scenarios considered in the observability analysis are outlined Table I, where $n, m \in \mathbb{N}$. In Table I, unknown means that no *a priori* knowledge about any of the states is available, whereas fully-known means that all the initial states are known. Thus, a fully-known receiver is one with known $\boldsymbol{x}_r(t_0)$, whereas a fully-known SOP is one with known $\boldsymbol{x}_s(t_0)$. On the other hand, partially-known means that only the initial position states are known. Thus, a partially-known receiver is one with known $\boldsymbol{r}_r(t_0)$, whereas a partially-known SOP is one with known $\boldsymbol{r}_s(t_0)$. For the cases of multiple SOPs, it is assumed that the SOPs are not colocated. Moreover, it is assumed that each SOP's classification, whether unknown, partially-known, or fully-known, is known to any receiver making use of that SOP.

TABLE I
COPNAV OBSERVABILITY ANALYSIS SCENARIOS CONSIDERED

Case	Receiver(s)	SOP(s)
1	1 Unknown	1 Unknown
2	1 Unknown	m Partially-known
3	1 Unknown	1 Fully-known
4	1 Unknown	1 Fully-known & 1 Partially-known
5	n Partially-known	1 Unknown
6	n Partially-known	m Partially-known
7	1 Partially-known	1 Fully-known
8	1 Fully-known	1 Unknown

C. Preliminary Facts

The following facts will be invoked in the observability proofs corresponding to Table I. First, the rank of an arbitrary matrix $\mathbf{A} \in \mathbb{R}^{m \times n}$ is the maximal number of linearly independent rows or columns; consequently, $\mathrm{rank}[\mathbf{A}] \leq \min\{m, n\}$. Second, when constructing $\boldsymbol{\mathcal{O}}_{\mathrm{NL}}$, one can stop calculating further derivatives of the output function at the first instance of linear dependence among the gradients, since after this point additional rows will not affect the rank of $\boldsymbol{\mathcal{O}}_{\mathrm{NL}}$. Third, the observable states in a COpNav environment, if any, can be found by computing the basis vectors spanning the null space of $\boldsymbol{\mathcal{O}}_{\mathrm{NL}}$, denoted $\mathcal{N}[\boldsymbol{\mathcal{O}}_{\mathrm{NL}}]$, and arranging the basis vectors into a matrix. The presence of a row of zeros in this matrix indicates that the corresponding state element is observable, since this state element is orthogonal to the unobservable subspace. Fourth, having prior knowledge about some of the COpNav environment states is equivalent to augmenting the observation vector with fictitious observations that are identical to these known states. For instance, an environment with a partially-known receiver and an unknown SOP can be associated with an observation vector $\boldsymbol{y} = [x_r, y_r, \rho]^{\mathsf{T}}$.

The remainder of this subsection discusses pertinent properties of the rows of $\boldsymbol{\mathcal{O}}_{\mathrm{NL}}$ in preparation for the observability proofs that will follow. Consider an environment with one receiver making a pseudorange observation on one SOP.

The vectors $\{\boldsymbol{f}_i\}_{i=0}^{r}$ corresponding to $\Sigma_{\rm NL}$ in (7) become $\boldsymbol{f}_0 = \dot{x}_r\boldsymbol{e}_1 + \dot{y}_r\boldsymbol{e}_2 + \dot{\delta t}_r\boldsymbol{e}_5 + \dot{\delta t}_s\boldsymbol{e}_9$, $\boldsymbol{f}_1 = \boldsymbol{e}_3$, and $\boldsymbol{f}_2 = \boldsymbol{e}_4$, where $\boldsymbol{e}_i$ is the standard basis vector consisting of a 1 in the ith element and zeros elsewhere. Consider the vector $\boldsymbol{h} = \left[x_r, y_r, \dot{x}_r, \dot{y}_r, \delta t_r, \dot{\delta t}_r, x_s, y_s, \delta t_s, \dot{\delta t}_s, \rho\right]^{\mathsf{T}}$.

It can be shown that the gradients of the zeroth-order Lie derivatives of $\{h_l(\boldsymbol{x})\}_{l=1}^{11}$ with respect to $\boldsymbol{f}_i$ are given by

$$\nabla_{\boldsymbol{x}}^{\mathsf{T}}\left[\mathfrak{L}_{\boldsymbol{f}_i}^{0} h_l(\boldsymbol{x})\right] = \begin{cases} g_1^0\cdot(\boldsymbol{e}_1^{\mathsf{T}} - \boldsymbol{e}_7^{\mathsf{T}}) + g_2^0\cdot(\boldsymbol{e}_2^{\mathsf{T}} - \boldsymbol{e}_8^{\mathsf{T}}) \\ \quad + c\cdot(\boldsymbol{e}_5^{\mathsf{T}} - \boldsymbol{e}_9^{\mathsf{T}}), & l = 11; \\ \boldsymbol{e}_l^{\mathsf{T}}, & \text{otherwise;} \end{cases}$$

for $i = 0, 1, 2$, where $g_1^0 \triangleq \frac{x_r - x_s}{\|\boldsymbol{r}_r - \boldsymbol{r}_s\|_2}$, $g_2^0 \triangleq \frac{y_r - y_s}{\|\boldsymbol{r}_r - \boldsymbol{r}_s\|_2}$.

The gradients of the first-order Lie derivatives are $\nabla_{\boldsymbol{x}}^{\mathsf{T}}\left[\mathfrak{L}_{\boldsymbol{f}_i}^{1} h_l(\boldsymbol{x})\right] = \boldsymbol{0}$, for $i = 1, 2$ and $\forall l$; and

$$\nabla_{\boldsymbol{x}}^{\mathsf{T}}\left[\mathfrak{L}_{\boldsymbol{f}_0}^{1} h_l(\boldsymbol{x})\right] = \begin{cases} \boldsymbol{e}_3^{\mathsf{T}}, & l = 1; \\ \boldsymbol{e}_4^{\mathsf{T}}, & l = 2; \\ \boldsymbol{e}_6^{\mathsf{T}}, & l = 5; \\ \boldsymbol{e}_{10}^{\mathsf{T}}, & l = 9; \\ g_1^1\cdot(\boldsymbol{e}_1^{\mathsf{T}} - \boldsymbol{e}_7^{\mathsf{T}}) + g_2^1\cdot(\boldsymbol{e}_2^{\mathsf{T}} - \boldsymbol{e}_8^{\mathsf{T}}) \\ \quad + g_3^1\,\boldsymbol{e}_3^{\mathsf{T}} + g_4^1\,\boldsymbol{e}_4^{\mathsf{T}} \\ \quad + c\cdot(\boldsymbol{e}_6^{\mathsf{T}} - \boldsymbol{e}_{10}^{\mathsf{T}}), & l = 11 \\ \boldsymbol{0}, & \text{otherwise;} \end{cases}$$

where $g_q^1 \triangleq \frac{\partial}{\partial\alpha}\left(\dot{x}_r\, g_1^0 + \dot{y}_r\, g_2^0\right)$, and $\alpha = x_r$ for $q = 1$, $\alpha = y_r$ for $q = 2$, $\alpha = \dot{x}_r$ for $q = 3$, and $\alpha = \dot{y}_r$ for $q = 4$.

The gradients of the second-order Lie derivatives are $\nabla_{\boldsymbol{x}}^{\mathsf{T}}\left[\mathfrak{L}_{\boldsymbol{f}_i}^{2} h_l(\boldsymbol{x})\right] = \boldsymbol{0}$, for $i = 1, 2$ and $\forall l$; and

$$\nabla_{\boldsymbol{x}}^{\mathsf{T}}\left[\mathfrak{L}_{\boldsymbol{f}_0}^{2} h_l(\boldsymbol{x})\right] = \begin{cases} g_1^2\cdot(\boldsymbol{e}_1^{\mathsf{T}} - \boldsymbol{e}_7^{\mathsf{T}}) + g_2^2\cdot(\boldsymbol{e}_2^{\mathsf{T}} - \boldsymbol{e}_8^{\mathsf{T}}) \\ \quad + g_3^2\,\boldsymbol{e}_3^{\mathsf{T}} + g_4^2\,\boldsymbol{e}_4^{\mathsf{T}}, & l = 11; \\ \boldsymbol{0}, & \text{otherwise;} \end{cases}$$

where $g_q^2 \triangleq \frac{\partial}{\partial\alpha}\left(\dot{x}_r\, g_1^1 + \dot{y}_r\, g_2^1\right)$, and $\alpha = x_r$ for $q = 1$, $\alpha = y_r$ for $q = 2$, $\alpha = \dot{x}_r$ for $q = 3$, and $\alpha = \dot{y}_r$ for $q = 4$,

$$\nabla_{\boldsymbol{x}}^{\mathsf{T}}\left[\mathfrak{L}_{\boldsymbol{f}_0\boldsymbol{f}_i}^{2} h_l(\boldsymbol{x})\right] = \begin{cases} g_\beta^2\cdot(\boldsymbol{e}_1^{\mathsf{T}} - \boldsymbol{e}_7^{\mathsf{T}}) \\ \quad + g_{\beta+1}^2\cdot(\boldsymbol{e}_2^{\mathsf{T}} - \boldsymbol{e}_8^{\mathsf{T}}), & l = 11; \\ \boldsymbol{0}, & \text{otherwise;} \end{cases}$$

where $\beta = 5$ if $i = 1$ and $\beta = 7$ if $i = 2$; and $g_\beta^2 \triangleq \frac{\partial}{\partial x_r} g_{i+2}^1$ and $g_{\beta+1}^2 \triangleq \frac{\partial}{\partial y_r} g_{i+2}^1$.

D. Observability Analysis

Theorem III.1. *A COpNav environment with one unknown receiver, without controlled maneuvers, and one unknown SOP has no observable states. Allowing controlled maneuvers makes the receiver velocity states observable.*

Proof: The observation vector is $\boldsymbol{y} = [\,\rho\,]$ and $\boldsymbol{x} \in \mathbb{R}^{10}$. Without control, the only linearly independent rows are $\left\{\nabla_{\boldsymbol{x}}^{\mathsf{T}}\left[\mathfrak{L}_{\boldsymbol{f}_0}^{p} h(\boldsymbol{x})\right], p = 0, \ldots, 4\right\}$; hence, $\operatorname{rank}[\boldsymbol{\mathcal{O}}_{\rm NL}] = 5$, and

$$\mathcal{N}[\boldsymbol{\mathcal{O}}_{\rm NL}] = \operatorname{span}\{\boldsymbol{n}_1,\, \boldsymbol{n}_2,\, \boldsymbol{n}_3,\, \boldsymbol{n}_4,\, \boldsymbol{n}_5\},$$

where $\boldsymbol{n}_1 \triangleq \boldsymbol{e}_1 + \boldsymbol{e}_7$, $\boldsymbol{n}_2 \triangleq \boldsymbol{e}_2 + \boldsymbol{e}_8$, $\boldsymbol{n}_3 \triangleq \boldsymbol{e}_5 + \boldsymbol{e}_9$, $\boldsymbol{n}_4 \triangleq \boldsymbol{e}_6 + \boldsymbol{e}_{10}$, $\boldsymbol{n}_5 \triangleq \sum_{i=1}^{4}\gamma_i\boldsymbol{e}_i$, and $\gamma_1 \triangleq \frac{-y_r + y_s}{\dot{x}_r}$, $\gamma_2 \triangleq \frac{x_r - x_s}{\dot{x}_r}$, $\gamma_3 \triangleq \frac{-\dot{y}_r}{\dot{x}_r}$, $\gamma_4 \triangleq 1$.

Allowing controlled maneuvers introduces an additional linearly independent row: $\left\{\nabla_{\boldsymbol{x}}^{\mathsf{T}}\left[\mathfrak{L}_{\boldsymbol{f}_0\boldsymbol{f}_i}^{2} h(\boldsymbol{x})\right], i = 1 \text{ or } 2\right\}$, yielding $\operatorname{rank}[\boldsymbol{\mathcal{O}}_{\rm NL}] = 6$ and removing $\boldsymbol{n}_5$ from $\mathcal{N}[\boldsymbol{\mathcal{O}}_{\rm NL}]$. ■

Theorem III.2. *A COpNav environment with one unknown receiver, without controlled maneuvers, and m partially-known SOPs has no observable states for $m = 1$. The receiver position and velocity states become observable for $m \geq 2$. Allowing controlled maneuvers makes the receiver position and velocity states observable $\forall\, m \geq 1$.*

Proof: The observation vector is $\boldsymbol{y} = [\boldsymbol{r}_{s_1}, \ldots, \boldsymbol{r}_{s_m}, \rho_{s_1}, \ldots, \rho_{s_m}]$ and $\boldsymbol{x} \in \mathbb{R}^{6+4m}$. Without control, and for $m = 1$, the only linearly independent rows are $\left\{\nabla_{\boldsymbol{x}}^{\mathsf{T}}\left[\mathfrak{L}_{\boldsymbol{f}_0}^{0} h_l(\boldsymbol{x})\right], l = 1, \ldots, 3; \nabla_{\boldsymbol{x}}^{\mathsf{T}}\left[\mathfrak{L}_{\boldsymbol{f}_0}^{p} h_3(\boldsymbol{x})\right], p = 1, \ldots, 4\right\}$; hence, $\operatorname{rank}[\boldsymbol{\mathcal{O}}_{\rm NL}] = 7$, and

$$\mathcal{N}[\boldsymbol{\mathcal{O}}_{\rm NL}] = \operatorname{span}\{\boldsymbol{n}_3,\, \boldsymbol{n}_4,\, \boldsymbol{n}_5\}.$$

For $m \geq 2$, the only linearly independent rows are $\left\{\nabla_{\boldsymbol{x}}^{\mathsf{T}}\left[\mathfrak{L}_{\boldsymbol{f}_0}^{0} h_l(\boldsymbol{x})\right], l = 1, \ldots, 3m; \nabla_{\boldsymbol{x}}^{\mathsf{T}}\left[\mathfrak{L}_{\boldsymbol{f}_0}^{1} h_l(\boldsymbol{x})\right], l = 2m+1, \ldots 3m\right\}$, with the following additional linearly independent rows:

- $m = 2$: $\left\{\nabla_{\boldsymbol{x}}^{\mathsf{T}}\left[\mathfrak{L}_{\boldsymbol{f}_0}^{p} h_l(\boldsymbol{x})\right], p = 2, 3, l = 5, 6\right\}$
- $m = 3$: $\left\{\nabla_{\boldsymbol{x}}^{\mathsf{T}}\left[\mathfrak{L}_{\boldsymbol{f}_0}^{2} h_l(\boldsymbol{x})\right], l = 7, 8, 9; \nabla_{\boldsymbol{x}}^{\mathsf{T}}\left[\mathfrak{L}_{\boldsymbol{f}_0}^{3} h_7(\boldsymbol{x})\right]\right\}$,
- $m \geq 4$: $\left\{\nabla_{\boldsymbol{x}}^{\mathsf{T}}\left[\mathfrak{L}_{\boldsymbol{f}_0}^{2} h_l(\boldsymbol{x})\right], l = 3m-4, \ldots, 3m\right\}$.

Hence, $\operatorname{rank}[\boldsymbol{\mathcal{O}}_{\rm NL}] = 4m + 4$, and

$$\mathcal{N}[\boldsymbol{\mathcal{O}}_{\rm NL}] = \operatorname{span}\{\boldsymbol{n}_6, \boldsymbol{n}_7\},$$

where $\boldsymbol{n}_6 \triangleq \boldsymbol{e}_5 + \sum_{i=1}^{m}\boldsymbol{e}_{5+4i}$ and $\boldsymbol{n}_7 \triangleq \boldsymbol{e}_7 + \sum_{i=1}^{m}\boldsymbol{e}_{6+4i}$.

Allowing controlled maneuvers, for $m \geq 1$, introduces an additional linearly independent row: $\left\{\nabla_{\boldsymbol{x}}^{\mathsf{T}}\left[\mathfrak{L}_{\boldsymbol{f}_0\boldsymbol{f}_i}^{2} h_{2m+1}(\boldsymbol{x})\right], i = 1 \text{ or } 2\right\}$, yielding $\operatorname{rank}[\boldsymbol{\mathcal{O}}_{\rm NL}] = 4m + 4$, and

$$\mathcal{N}[\boldsymbol{\mathcal{O}}_{\rm NL}] = \operatorname{span}\{\boldsymbol{n}_6,\, \boldsymbol{n}_7\}.$$ ■

Theorem III.3. *A COpNav environment with one unknown receiver, without controlled maneuvers, and one fully-known SOP only has observable the receiver clock bias and drift states. Allowing controlled maneuvers makes all the states observable.*

Proof: The observation vector is $\boldsymbol{y} = [\,\boldsymbol{x}_s, \rho\,]$ and $\boldsymbol{x} \in \mathbb{R}^{10}$. Without control, the only linearly independent rows are $\left\{\nabla_{\boldsymbol{x}}^{\mathsf{T}}\left[\mathfrak{L}_{\boldsymbol{f}_0}^{0} h_l(\boldsymbol{x})\right], l = 1, \ldots, 5; \nabla_{\boldsymbol{x}}^{\mathsf{T}}\left[\mathfrak{L}_{\boldsymbol{f}_0}^{p} h_5(\boldsymbol{x})\right], p = 1, \ldots, 4\right\}$; hence, $\operatorname{rank}[\boldsymbol{\mathcal{O}}_{\rm NL}] = 9$, and

$$\mathcal{N}[\boldsymbol{\mathcal{O}}_{\rm NL}] = \operatorname{span}\{\boldsymbol{n}_5\}.$$

Allowing controlled maneuvers introduces an additional linearly independent row: $\left\{\nabla_{\boldsymbol{x}}^{\mathsf{T}}\left[\mathfrak{L}_{\boldsymbol{f}_0\boldsymbol{f}_i}^{2} h_5(\boldsymbol{x})\right], i = 1 \text{ or } 2\right\}$, yielding $\operatorname{rank}[\boldsymbol{\mathcal{O}}_{\rm NL}] = 10$. ■

Theorem III.4. *A COpNav environment with one unknown receiver, without controlled maneuvers, one fully-known SOP, and one partially-known SOP is fully-observable. Allowing controlled maneuvers does not affect observability.*

Proof: The observation vector is $\boldsymbol{y} = [\,\boldsymbol{x}_{s_1}, \boldsymbol{r}_{s_2}, \rho_{s_1}, \rho_{s_2}\,]$ and $\boldsymbol{x} \in \mathbb{R}^{14}$. Without control, the only linearly independent rows are $\left\{\nabla_{\boldsymbol{x}}^{\mathsf{T}}\left[\mathfrak{L}_{\boldsymbol{f}_0}^0 h_l(\boldsymbol{x})\right], l = 1,\ldots,8; \nabla_{\boldsymbol{x}}^{\mathsf{T}}\left[\mathfrak{L}_{\boldsymbol{f}_0}^p h_l(\boldsymbol{x})\right], p = 1,\ldots,3,\ l = 7,8\right\}$, and $\operatorname{rank}[\boldsymbol{\mathcal{O}}_{\mathrm{NL}}] = 14$. Allowing controlled maneuvers does not add linearly independent rows. ■

Theorem III.5. *A COpNav environment with n partially-known receivers, without controlled maneuvers, and one unknown SOP only has observable the receivers' velocity states and the SOP's position states. Allowing controlled maneuvers does not affect observability.*

Proof: The observation vector is $\boldsymbol{y} = [\boldsymbol{r}_{r_1}, \ldots, \boldsymbol{r}_{r_n}, \rho_{r_1}, \ldots, \rho_{r_n}]$ and $\boldsymbol{x} \in \mathbb{R}^{6n+4}$. Without control, the only linearly independent rows are $\left\{\nabla_{\boldsymbol{x}}^{\mathsf{T}}\left[\mathfrak{L}_{\boldsymbol{f}_0}^p h_l(\boldsymbol{x})\right], p = 0,1, l = 1,\ldots,3n\right\}$, with the following additional linearly independent rows:

- $n = 1$: $\left\{\nabla_{\boldsymbol{x}}^{\mathsf{T}}\left[\mathfrak{L}_{\boldsymbol{f}_0}^p h_3(\boldsymbol{x})\right], p = 2,3\right\}$,
- $n \geq 2$: $\left\{\nabla_{\boldsymbol{x}}^{\mathsf{T}}\left[\mathfrak{L}_{\boldsymbol{f}_0}^2 h_l(\boldsymbol{x})\right], l = 2n+1, 2n+2\right\}$.

Hence, $\operatorname{rank}[\boldsymbol{\mathcal{O}}_{\mathrm{NL}}] = 6n+2$, and

$$\mathcal{N}[\boldsymbol{\mathcal{O}}_{\mathrm{NL}}] = \operatorname{span}\left\{\boldsymbol{e}_5 + \sum_{i=1}^{n} \boldsymbol{e}_{5+6i},\ \boldsymbol{e}_6 + \sum_{i=1}^{n} \boldsymbol{e}_{6+6i}\right\}.$$

Allowing controlled maneuvers does not improve the rank any further, since the control inputs will introduce additional rows into $\boldsymbol{\mathcal{O}}_{\mathrm{NL}}$ whose columns are linearly independent according to: $\boldsymbol{\mathcal{O}}_{6n+3} = -\sum_{i=0}^{n-1} \boldsymbol{\mathcal{O}}_{5+6i}$ and $\boldsymbol{\mathcal{O}}_{6n+4} = -\sum_{i=0}^{n-1} \boldsymbol{\mathcal{O}}_{6+6i}$, where $\boldsymbol{\mathcal{O}}_i$ corresponds to the ith column of $\boldsymbol{\mathcal{O}}_{\mathrm{NL}}$. ■

Theorem III.6. *A COpNav environment with n partially-known receivers, without controlled maneuvers, and m partially-known SOPs only has observable the receivers' velocity states. Allowing controlled maneuvers does not affect observability.*

Proof: The observation vector is $\boldsymbol{y} = [\boldsymbol{r}_{r_1}, \ldots, \boldsymbol{r}_{r_n}, \boldsymbol{r}_{s_1}, \ldots, \boldsymbol{r}_{s_m}, \rho_{r_1,s_1}, \ldots, \rho_{r_n,s_m}]$ and $\boldsymbol{x} \in \mathbb{R}^{6n+4m}$. Without control, the only linearly independent rows are $\left\{\nabla_{\boldsymbol{x}}^{\mathsf{T}}\left[\mathfrak{L}_{\boldsymbol{f}_0}^0 h_l(\boldsymbol{x})\right], l = 1,\ldots,2n+2m+nm; \nabla_{\boldsymbol{x}}^{\mathsf{T}}\left[\mathfrak{L}_{\boldsymbol{f}_0}^1 h_l(\boldsymbol{x})\right], l = 2m+1,\ldots,4n+4m-nm-2\right\}$; hence, $\operatorname{rank}[\boldsymbol{\mathcal{O}}_{\mathrm{NL}}] = 6n+4m-2$, and

$$\mathcal{N}[\boldsymbol{\mathcal{O}}_{\mathrm{NL}}] = \operatorname{span}\Bigg\{\boldsymbol{e}_{6n+4m-1} + \sum_{l=1}^{n} \boldsymbol{e}_{6l-1} + \sum_{l=0}^{m-2} \boldsymbol{e}_{6n+4l+3},\ \boldsymbol{e}_{6n+4m} + \sum_{l=1}^{n} \boldsymbol{e}_{6l} + \sum_{l=0}^{m-2} \boldsymbol{e}_{6n+4l+4}\Bigg\},$$

Allowing controlled maneuvers does not improve the rank any further, since the control inputs will introduce additional rows into $\boldsymbol{\mathcal{O}}_{\mathrm{NL}}$ whose columns are linearly independent according to: $\boldsymbol{\mathcal{O}}_{6n+4m-1} = -\left[\sum_{l=1}^{n} \boldsymbol{\mathcal{O}}_{6l-1} + \sum_{l=0}^{m-2} \boldsymbol{\mathcal{O}}_{6n+4l+3}\right]$ and $\boldsymbol{\mathcal{O}}_{6n+4m} = -\left[\sum_{l=1}^{n} \boldsymbol{\mathcal{O}}_{6l} + \sum_{l=0}^{m-2} \boldsymbol{\mathcal{O}}_{6n+4l+4}\right]$. ■

Theorem III.7. *A COpNav environment with one partially-known receiver, without controlled maneuvers, and one fully-known SOP is fully-observable. Allowing controlled maneuvers does not affect observability.*

Proof: The observation vector is $\boldsymbol{y} = [\boldsymbol{r}_r, \boldsymbol{x}_s, \rho]$ and $\boldsymbol{x} \in \mathbb{R}^{10}$. Without control, the only linearly independent rows are $\left\{\nabla_{\boldsymbol{x}}^{\mathsf{T}}\left[\mathfrak{L}_{\boldsymbol{f}_0}^0 h_l(\boldsymbol{x})\right], l = 1,\ldots,7; \nabla_{\boldsymbol{x}}^{\mathsf{T}}\left[\mathfrak{L}_{\boldsymbol{f}_0}^1 h_l(\boldsymbol{x})\right], l = 1,2,7\right\}$ and $\operatorname{rank}[\boldsymbol{\mathcal{O}}_{\mathrm{NL}}] = 10$, i.e., full-rank. ■

Theorem III.8. *A COpNav environment with one fully-known receiver, without controlled maneuvers, and one unknown SOP is fully-observable. Allowing controlled maneuvers does not affect observability.*

Proof: The observation vector is $\boldsymbol{y} = [\boldsymbol{r}_r, \rho\,]$ and $\boldsymbol{x} \in \mathbb{R}^{10}$. Without control, the only linearly independent rows are $\left\{\nabla_{\boldsymbol{x}}^{\mathsf{T}}\left[\mathfrak{L}_{\boldsymbol{f}_0}^0 h_l(\boldsymbol{x})\right], l = 1,\ldots,7; \nabla_{\boldsymbol{x}}^{\mathsf{T}}\left[\mathfrak{L}_{\boldsymbol{f}_0}^1 h_l(\boldsymbol{x})\right], l = 1,2,7\right\}$ and $\operatorname{rank}[\boldsymbol{\mathcal{O}}_{\mathrm{NL}}] = 10$, i.e., full-rank.

■

Table II summarizes the observability results. It is concluded that a planar COpNav environment comprising n receivers with velocity random walk dynamics making pseudorange observations on m terrestrial SOPs is fully-observable if the initial states of at least: (i) one receiver is fully-known, (ii) one receiver is partially-known and one SOP is fully-known, or (iii) one SOP is fully-known and one SOP is partially-known. If the receivers control their maneuvers in the form of acceleration commands, the environment is fully-observable if the initial states of at least: (i) one receiver is fully-known or (ii) one SOP is fully-known.

TABLE II
COPNAV OBSERVABILITY ANALYSIS RESULTS: OBSERVABLE STATES

Case	Without Control	With Control
1	none	$\dot{x}_r$, $\dot{y}_r$
2	$m = 1$: none $m \geq 2$: x_r, y_r, $\dot{x}_r$, $\dot{y}_r$	$m \geq 1$: x_r, y_r, $\dot{x}_r$, $\dot{y}_r$
3	δt_r, $\dot{\delta} t_r$	all
4	all	all
5	$\dot{x}_{r_i}$, $\dot{y}_{r_i}$, x_s, y_s, $i = 1,\ldots,n$	$\dot{x}_{r_i}$, $\dot{y}_{r_i}$, x_s, y_s, $i = 1,\ldots,n$
6	$\dot{x}_{r_i}$, $\dot{y}_{r_i}$, $i = 1,\ldots,n$	$\dot{x}_{r_i}$, $\dot{y}_{r_i}$, $i = 1,\ldots,n$
7	all	all
8	all	all

IV. RECEDING HORIZON RECEIVER TRAJECTORY OPTIMIZATION

This section presents the proposed receding horizon receiver trajectory optimization for optimal information gathering in an OpNav environment comprising a single receiver and multiple SOPs. Here, the information gathered by the receiver about the environment is locally fused and utilized to prescribe the receiver's trajectory. For the case of multiple receivers, various decision making and information fusion architectures arise, e.g., centralized, decentralized, and hierarchical [20]. The forthcoming discussion assumes that the receiver either has full knowledge of the initial state of one anchor SOP or its own initial state; hence, making the environment fully observable in accordance with the conditions established in Section III.

In receding horizon trajectory optimization, at a particular time step, a multi-step look-ahead optimal control sequence is computed. However, only the first step of this sequence is

applied, whereas the rest of the sequence is discarded. This is motivated by the fact that at the next time step, a new measurement becomes available, which contains information that is used to refine the optimal trajectory.

The proposed receding horizon trajectory optimization loop is illustrated in Fig. 1. At a particular time step t_k, the pseudorange observations made by the receiver on the SOPs in the environment, $\boldsymbol{z}(t_k) \triangleq [z_1(t_k), \ldots, z_m(t_k)]^{\mathsf{T}}$, are fused through an estimator, an extended Kalman filter (EKF) in this case, which produces a state estimate $\hat{\boldsymbol{x}}(t_k|t_k)$ and an associated estimation error covariance $\mathbf{P}(t_k|t_k)$. The estimate and associated covariance are fed into a receding horizon optimal control solver, which solves for the optimal admissible N-step look-ahead control actions $\boldsymbol{U}_{t_k}^N$, which are defined as $\left(\boldsymbol{U}_{t_k}^N\right)^\star \triangleq \{\boldsymbol{u}^\star(t_{k+j}),\, j=0,\ldots,N-1\}$ to minimize the D-optimality cost functional $\mathcal{J}$, subject to the OpNav dynamics and observation model Σ_{OpNav} along with velocity and acceleration constraints. The D-optimality criterion is proportional to the volume of the estimation error uncertainty ellipsoid [19] and was demonstrated in [18] to yield less estimation error than the A-optimality and E-optimality criteria. In Fig. 1, $v_{r,\max}$ and $a_{r,\max}$ represent the maximum speed and acceleration, respectively, with which the receiver can move.

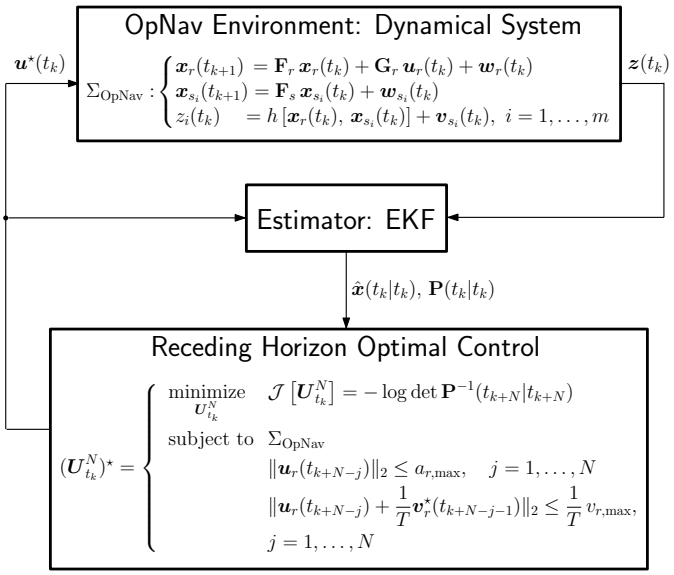

Fig. 1. N-step look-ahead receding horizon receiver motion planning loop

Note that if $N = 1$, the receding horizon trajectory optimization problem reduces to greedy optimization. To evaluate the N-step estimation error covariance, $\mathbf{P}(t_{k+N}|t_{k+N})$, the zero future innovations assumption, namely $\tilde{\boldsymbol{z}}(t_{j+1}) \triangleq \boldsymbol{z}(t_{j+1}) - \boldsymbol{h}\,[\hat{\boldsymbol{x}}(t_{j+1}|t_j)] \equiv 0$, for $j = k, \ldots, k+N-1$, will be invoked [16]. Once the optimal N-step look-ahead control actions $\left(\boldsymbol{U}_{t_k}^N\right)^\star$ are found, only the first control action $\boldsymbol{u}^\star(t_k)$ is applied, whereas the rest of the control actions $\{\boldsymbol{u}^\star(t_j)\}_{j=k+1}^{k+N-1}$ are discarded. A single iteration of the proposed algorithm for finding the receding horizon optimal receiver trajectory is outlined in Algorithm 1.

One drawback of receding horizon trajectory optimization is repeated invoking of the zero-innovation assumption. Another drawback is increased computational burden. Fig. 2 illustrates the cascade of feasibility regions that should be considered as the horizon is increased. In particular, each point in the black shaded region corresponding to the feasibility region of the first-step look-ahead has an associated feasibility region of its own signifying the feasible maneuvers the receiver could take for the second-step. The number of optimization variables for an N-step look-ahead problem are $2N$. Denoting the number of feasible maneuvers in a particular time step t_j by n_j, it is easy to see that an exhaustive search-type algorithm has a computational burden $\mathcal{O}\left(\prod_{j=1}^N n_j\right)$.

Algorithm 1 N-step look-ahead receding horizon trajectory optimization

Given: $\hat{\boldsymbol{x}}(t_k|t_k)$, $\mathbf{P}(t_k|t_k)$, N
for $j = k, \ldots, k+N-1$ **find**

$$\hat{\boldsymbol{x}}(t_{j+1}|t_j) = \mathbf{F}\hat{\boldsymbol{x}}(t_j|t_j) + \mathbf{G}\boldsymbol{u}(t_j)$$
$$\mathbf{H}(t_{j+1}) = \left.\frac{\partial \boldsymbol{h}[\boldsymbol{x}_r(t_{j+1}), \boldsymbol{x}_s(t_{j+1})]}{\partial \boldsymbol{x}}\right|_{\boldsymbol{x}=\hat{\boldsymbol{x}}(t_{j+1}|t_j)}$$
$$\mathbf{P}(t_{j+1}|t_j) = \mathbf{F}\mathbf{P}(t_j|t_j)\mathbf{F}^{\mathsf{T}} + \mathbf{Q}$$
$$\mathbf{S}(t_{j+1}) = \mathbf{H}(t_{j+1})\mathbf{P}(t_{j+1}|t_j)\mathbf{H}^{\mathsf{T}}(t_{j+1}) + \mathbf{R}$$
$$\mathbf{W}(t_{j+1}) = \mathbf{P}(t_{j+1}|t_j)\mathbf{H}^{\mathsf{T}}(t_{j+1})\mathbf{S}^{-1}(t_{j+1})$$
$$\mathbf{P}(t_{j+1}|t_{j+1}) = \mathbf{P}(t_{j+1}|t_j) - \mathbf{W}(t_{j+1})\mathbf{S}(t_{j+1})\mathbf{W}^{\mathsf{T}}(t_{j+1})$$
$$\hat{\boldsymbol{x}}(t_{j+1}|t_{j+1}) \equiv \hat{\boldsymbol{x}}(t_{j+1}|t_j)$$

end for
Solve:

$$\underset{\boldsymbol{U}_{t_k}^N}{\text{minimize}} \quad \mathcal{J}\left[\boldsymbol{U}_{t_k}^N\right] = -\log\det\mathbf{P}^{-1}(t_{k+N}|t_{k+N})$$

subject to Σ_{OpNav}

$$\|\boldsymbol{u}_r(t_{k+N-j})\|_2 \le a_{r,\max}, \quad j=1,\ldots,N$$
$$\left\|\boldsymbol{u}_r(t_{k+N-j}) + \frac{\boldsymbol{v}_r^\star(t_{k+N-j-1})}{T}\right\|_2 \le \frac{v_{r,\max}}{T}, \quad j=1,\ldots,N$$

Apply: $\boldsymbol{u}^\star(t_k)$
Discard: $\{\boldsymbol{u}^\star(t_{k+1}), \ldots, \boldsymbol{u}^\star(t_{k+N-1})\}$

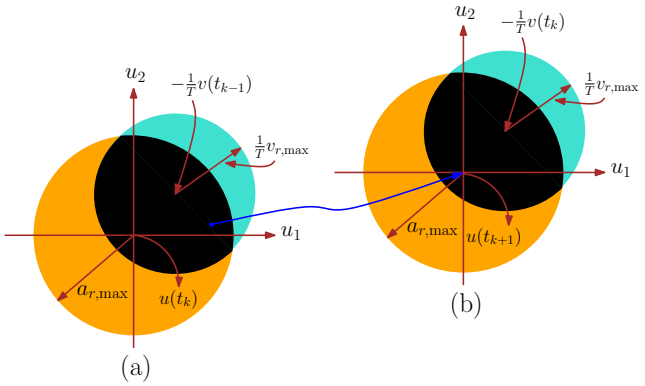

Fig. 2. Cascade of feasibility regions for two-step look-ahead horizon. The two disks in (a) represent the acceleration and velocity constraints for the first-step look-ahead. The disks intersection (black shaded area) are the receiver feasible maneuvers. Each point in this feasibility region is associated with another feasibility region in (b) representing the feasible maneuvers for the second-step look-ahead.

V. Simulation Results

This section presents simulation results to demonstrate the limitations and effectiveness of receding horizon trajectory optimization versus greedy. An OpNav environment comprising a receiver and four SOPs, labeled $\{\mathrm{SOP}_i\}_{i=1}^4$, was simulated according to the settings presented in Table III. The receiver's and SOPs' clocks were assumed to be temperature-compensated and oven-controlled crystal oscillators (TCXO and OCXOs), respectively. For purposes of numerical stability, the clock error states were defined to be $c\delta t$ and $c\dot{\delta t}$. Two receiver modes of operation were considered, corresponding to the two observability conditions established in Section III: (i) simultaneous receiver localization and signal landscape mapping in an environment with one fully-known "anchor" SOP and three unknown SOPs, and (ii) signal landscape mapping in an environment with four unknown SOPs and a fully-known receiver.

TABLE III
Simulation Settings

Parameter	Value
$\boldsymbol{x}_{s_1}(t_0)$	$[\,0,\,150,\,10,\,0.1\,]^\mathsf{T}$
$\boldsymbol{x}_{s_2}(t_0)$	$[\,100,\,-150,\,20,\,0.2\,]^\mathsf{T}$
$\boldsymbol{x}_{s_3}(t_0)$	$[\,200,\,200,\,30,\,0.3\,]^\mathsf{T}$
$\boldsymbol{x}_{s_4}(t_0)$	$[\,-150,\,50,\,40,\,0.4\,]^\mathsf{T}$
$\{h_{0,r},\, h_{-2,r}\}$	$\{2\times10^{-19},\, 2\times10^{-20}\}$
$\left\{h_{0,s_j},\, h_{-2,s_j}\right\}$	$\{8\times10^{-20},\, 4\times10^{-23}\},\ \ j=1,\ldots,4$
$\tilde{q}_x,\, \tilde{q}_y$	$0.1\,(\mathrm{m/s^2})^2$
r	$\{250,\,300,\,350\}\ \mathrm{m}^2$
$\{v_{\max},\, a_{\max}\}$	$\left\{10\,\mathrm{m/s},\, 3\,\mathrm{m/s^2}\right\}$
T	$0.2\,\mathrm{s}$

Three sets of simulations were performed for three different observation noise intensities r. Four receiver trajectories per noise intensity were generated: a random trajectory, a greedy trajectory (i.e., $N=1$), and two receding horizon trajectories with $N=2$ and $N=3$. The random trajectory was generated by choosing at every time step a feasible maneuver at random, while the greedy and receding horizon trajectories were generated through Algorithm 1. The optimal solution was found through an exhaustive search over the feasibility region depicted in Fig. 2. To this end, the acceleration space was gridded with spacing $\delta u_x = \delta u_y = 1\,\mathrm{m/s^2}$ and the extreme points of the two disks corresponding to the acceleration and velocity constraints were gridded with an angular spacing of 0.15 rad. This resulted in around 35^N feasible maneuvers on average at a particular time step. For meaningful comparison, the same initial state estimates and process and observation noise realization time histories were used to generate the four receiver trajectories. Several MC-based runs were conducted for each noise intensity with randomized initial state estimates and noise realization time histories.

A. Case 1: Simultaneous Receiver Localization and Signal Landscape Mapping with One Known Anchor SOP

The receiver was assumed to have the initial state $\boldsymbol{x}_r(t_0) = [\,0,\,0,\,10,\,0,\,100,\,10\,]^\mathsf{T}$ and the known anchor SOP was assumed to be SOP_1. The initial estimates for the receiver and the three SOPs were generated according to $\hat{\boldsymbol{x}}_r(t_0|t_0) \sim \mathcal{N}\left[\boldsymbol{x}_r(t_0), \mathbf{P}_r(t_0|t_0)\right]$ and $\hat{\boldsymbol{x}}_{s_i}(t_0|t_0) \sim \mathcal{N}\left[\boldsymbol{x}_{s_i}(t_0), \mathbf{P}_{s_i}(t_0|t_0)\right],\ i = 2,3,4$, with initial estimation error covariance matrices $\mathbf{P}_r(t_0|t_0) = (10^4)\cdot\mathrm{diag}\left[\,1,\,1,\,1,\,1,\,1,\,10^{-2}\,\right]$ and $\mathbf{P}_{s_i}(t_0|t_0) = (10^4)\cdot\mathrm{diag}\left[\,1,\,1,\,1,\,10^{-2}\,\right]$. To assess the localization accuracy and signal landscape map quality, the natural logarithm of the posterior estimation error covariance determinant, namely $\log\det\left[\mathbf{P}(t_{k+1}|t_{k+1})\right]$, was adopted.

The resulting receiver trajectories for $r = 250\,\mathrm{m}^2$ and a particular run are illustrated in Fig. 3. The resulting localization and signal landscape map uncertainties for $r \in \{\,250,\,300,\,350\,\}\ \mathrm{m}^2$ and the same run are plotted in Fig. 4-6. The $\log\det\left[\mathbf{P}^\star(t_{k+1}|t_{k+1})\right]$ plots exhibited a similar behavior for various MC runs. The reduction in receiver localization and signal landscape map estimation uncertainty for the receding horizon approaches over the greedy approach at the end of the simulation time is averaged over ten MC runs and is tabulated in Table IV.

TABLE IV
Average % reduction in receiver localization and signal landscape map estimation uncertainty for N-step look-ahead receding horizon over greedy and various observation noise intensities, r

N	$r=250$	$r=300$	$r=350$
2	14.19	7.51	-8.03
3	29.63	20.95	6.28

B. Case 2: Signal Landscape Mapping with a Known Receiver

The receiver was assumed to have an initial known state of $\boldsymbol{x}_r(t_0) = [\,0,\,0,\,0,\,0,\,100,\,10\,]^\mathsf{T}$. The initial estimates for the the four SOPs were generated according to $\hat{\boldsymbol{x}}_{s_i}(t_0|t_0) \sim \mathcal{N}\left[\boldsymbol{x}_{s_i}(t_0), \mathbf{P}_{s_i}(t_0|t_0)\right],\ i = 1,\ldots,4$, with initial estimation error covariance matrices $\mathbf{P}_{s_i}(t_0|t_0) = (10^4)\cdot\mathrm{diag}\left[\,1,\,1,\,1,\,10^{-2}\,\right]$. To assess the signal landscape map quality, $\log\det\left[\mathbf{P}(t_{k+1}|t_{k+1})\right]$ was adopted.

The resulting receiver trajectories for $r = 250\,\mathrm{m}^2$ and a particular run are illustrated in Fig. 7. The resulting signal landscape map uncertainty for $r \in \{\,250,\,300,\,350\,\}\ \mathrm{m}^2$ and the same run are plotted in Fig. 8-10. The $\log\det\left[\mathbf{P}^\star(t_{k+1}|t_{k+1})\right]$ plots exhibited a similar behavior for various MC runs. The reduction in signal landscape map estimation uncertainty for the receding horizon approaches over the greedy approach at the end of the simulation time is averaged over ten MC runs and is tabulated in Table V.

TABLE V
Average % reduction in signal landscape map estimation uncertainty for N-step look-ahead receding horizon over greedy and various observation noise intensities, r

N	$r=250$	$r=300$	$r=350$
2	94.69	55.56	43.61
3	135.51	78.46	52.63

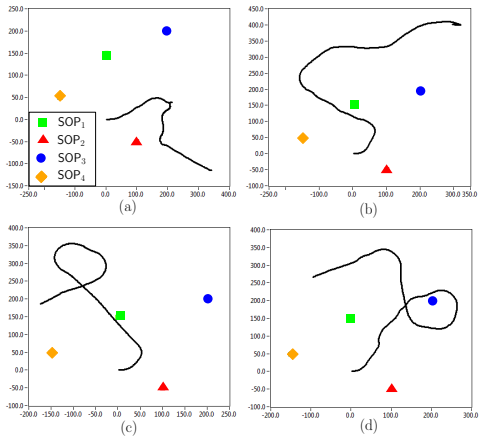

Fig. 3. Case 1: receiver trajectories due to (a) random, (b) optimal greedy, (c) optimal two-step look-ahead, and (d) optimal three-step look-ahead

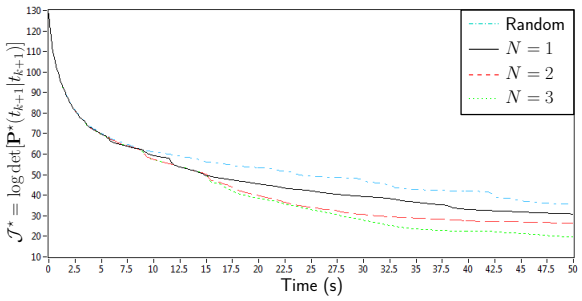

Fig. 4. Localization & signal landscape map uncertainty due to random receiver maneuvers and optimal N-step look-ahead with $r = 250$

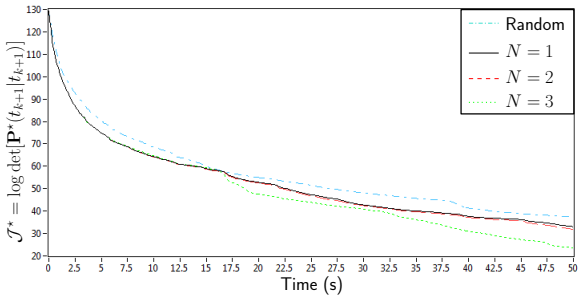

Fig. 5. Localization & signal landscape map uncertainty due to random receiver maneuvers and optimal N-step look-ahead with $r = 300$

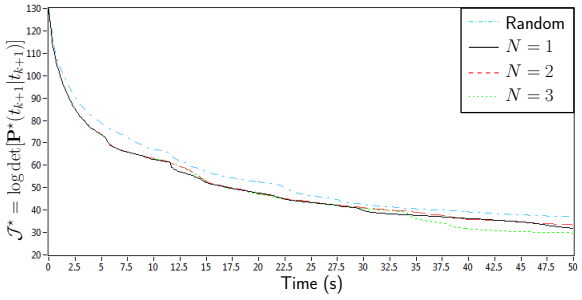

Fig. 6. Localization & signal landscape map uncertainty due to random receiver maneuvers and optimal N-step look-ahead with $r = 350$

C. Simulation Results Discussion

The following conclusions can be drawn from the presented simulations. First, greedy motion planning and receding horizon trajectory optimization yielded superior results to random trajectories. Second, receding horizon trajectory optimization outperformed greedy motion planning. However, this superiority came at the expense of increased computational burden. In particular, at each time step, the greedy motion planning required the computation of around 35 functionals of the posterior estimation error covariance matrix, corresponding to each feasible maneuver. The receding horizon trajectory optimization, on the other hand, required the computation of around 35^N functionals at each time step, where $N = 2, 3$. Third, the superiority of receding horizon over greedy depends on the observation noise intensity – the larger the observation noise, the less advantage the receding horizon strategy has. In fact, for large enough observation noise, receding horizon yields nearly identical (or slightly worse) performance than greedy. Fourth, for the same simulation settings, the improvements gained from receding horizon over greedy were more significant whenever the receiver had *a priori* knowledge about its own state and was tasked with signal landscape mapping, over the case where the receiver had no *a priori* knowledge about its state and was tasked with simultaneous receiver localization and signal landscape mapping.

VI. Conclusions

This paper studied the problem of multi-step look-ahead (receding horizon) receiver trajectory optimization for optimal information gathering in OpNav environments. To this end, it was first shown that allowing receivers to actively control their maneuvers reduces the required *a priori* knowledge about the environment for complete observability. In particular, it was shown that a planar COpNav environment comprising multiple receivers with velocity random walk dynamics making pseudorange observations on multiple terrestrial SOPs is fully observable if the initial states of at least: (i) one receiver is fully-known, (ii) one receiver is partially-known and one SOP is fully-known, or (iii) one SOP is fully-known and one SOP is partially-known. If the receivers control their maneuvers in the form of acceleration commands, the environment is fully-observable if the initial states of at least: (i) one receiver is fully-known or (ii) one SOP is fully-known. Furthermore, random receiver trajectories, greedy trajectories, and receding horizon trajectories were compared. It was demonstrated that optimal greedy and receding horizon receiver motion planning yielded higher fidelity signal landscape maps and more accurate receiver localization than random receiver trajectories. Moreover, the improvements gained from receding horizon over greedy were more prominent for the case of signal landscape mapping with a known receiver over the case of simultaneous receiver localization and signal landscape mapping with a known anchor SOP. It was demonstrated that while the receding horizon strategy outperformed the greedy method, the receding horizon strategy became less advantageous as the environment uncertainty in the form of observation noise intensity was increased. Future work will study convexity properties of the optimal motion planning strategy.

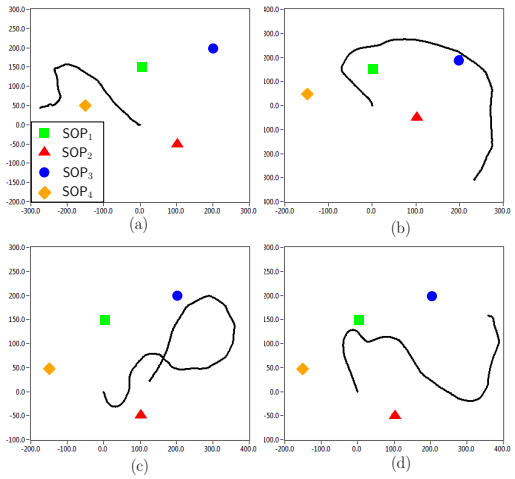

Fig. 7. Case 2: receiver trajectories due to (a) random, (b) optimal greedy, (c) optimal two-step look-ahead, and (d) optimal three-step look-ahead

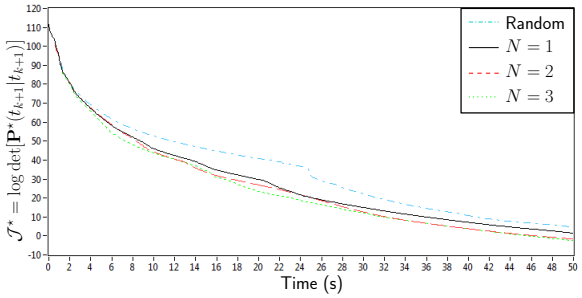

Fig. 8. Signal landscape map uncertainty due to random receiver maneuvers and optimal N-step look-ahead with $r = 250$

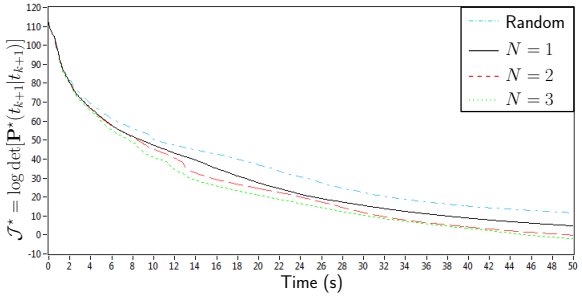

Fig. 9. Signal landscape map uncertainty due to random receiver maneuvers and optimal N-step look-ahead with $r = 300$

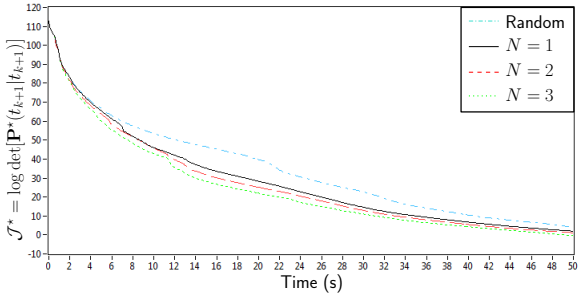

Fig. 10. Signal landscape map uncertainty due to random receiver maneuvers and optimal N-step look-ahead with $r = 350$

ACKNOWLEDGMENT

The authors would like to thank Jahshan Bhatti for helpful discussions.

REFERENCES

[1] K. Pesyna, Z. Kassas, J. Bhatti, and T. Humphreys, "Tightly-coupled opportunistic navigation for deep urban and indoor positioning," in *Proceedings of the ION GNSS*, vol. 1, September 2011, pp. 3605–3617.

[2] C. Yang, T. Nguyen, E. Blasch, and D. Qiu, "Assessing terrestrial wireless communications and broadcast signals as signals of opportunity for positioning and navigation," in *Proceedings of the ION GNSS*, September 2012, pp. 3814–3824.

[3] P. Thevenon, S. Damien, O. Julien, C. Macabiau, M. Bousquet, L. Ries, and S. Corazza, "Positioning using mobile TV based on the DVB-SH standard," *NAVIGATION, Journal of the Institute of Navigation*, vol. 58, no. 2, pp. 71–90, 2011.

[4] K. Pesyna, Z. Kassas, and T. Humphreys, "Constructing a continuous phase time history from TDMA signals for opportunistic navigation," in *Proceedings of IEEE/ION Position Location and Navigation Symposium*, April 2012, pp. 1209–1220.

[5] K. Kauffman, J. Raquet, Y. Morton, and D. Garmatyuk, "Real-time UWB-OFDM radar-based navigation in unknown terrain," *IEEE Transactions on Aerospace and Electronic Systems*, vol. 49, no. 3, pp. 1453–1466, 2013.

[6] Z. Kassas, "Collaborative opportunistic navigation," *IEEE Aerospace and Electronic Systems Magazine*, vol. 28, no. 6, pp. 38–41, June 2013.

[7] H. Durrant-Whyte and T. Bailey, "Simultaneous localization and mapping: part I," *IEEE Robotics and Automation Magazine*, vol. 13, no. 2, pp. 99–110, June 2006.

[8] T. Bailey and H. Durrant-Whyte, "Simultaneous localization and mapping: part II," *IEEE Robotics and Automation Magazine*, vol. 13, no. 3, pp. 108–117, September 2006.

[9] Z. Kassas and T. Humphreys, "Observability analysis of opportunistic navigation with pseudorange measurements," in *Proceedings of AIAA Guidance, Navigation, and Control Conference*, vol. 1, August 2012, pp. 4760–4775.

[10] ——, "Observability analysis of collaborative opportunistic navigation with pseudorange measurements," *IEEE Transactions on Intelligent Transportation Systems*, 2013, in press.

[11] ——, "Observability and estimability of collaborative opportunistic navigation with pseudorange measurements," in *Proceedings of the ION GNSS*, September 2012, pp. 621–630.

[12] J. Passerieux and D. V. Cappel, "Optimal observer maneuver for bearings-only tracking," *IEEE Transactions on Aerospace and Electronic Systems*, vol. 34, no. 3, pp. 777–788, July 1998.

[13] Y. Oshman and P. Davidson, "Optimization of observer trajectories for bearings-only target localization," *IEEE Transactions on Aerospace and Electronic Systems*, vol. 35, no. 3, pp. 892–902, July 1999.

[14] S. Ponda, R. Kolacinski, and E. Frazzoli, "Trajectory optimization for target localization using small unmanned aerial vehicles," in *Proceedings of AIAA Guidance, Navigation, and Control Conference*, August 2009, pp. 1209–1220.

[15] H. Feder, J. Leonard, and C. Smith, "Adaptive mobile robot navigation and mapping," *International Journal of Robotics Research*, vol. 18, no. 7, pp. 650–668, July 1999.

[16] C. Leung, S. Huang, N. Kwok, and G. Dissanayake, "Planning under uncertainty using model predictive control for information gathering," *Robotics and Autonomous Systems*, vol. 54, no. 11, pp. 898–910, November 2006.

[17] M. Bryson and S. Sukkarieh, "Observability analysis and active control for airborne SLAM," *IEEE Transactions on Aerospace and Electronic Systems*, vol. 44, no. 1, pp. 261–280, January 2008.

[18] Z. Kassas and T. Humphreys, "Motion planning for optimal information gathering in opportunistic navigation systems," in *Proceedings of AIAA Guidance, Navigation, and Control Conference*, August 2013, pp. 4551–4565.

[19] D. Uciński, *Optimal Measurement Methods for Distributed Parameter System Identification*. CRC Press, 2005.

[20] Z. Kassas and T. Humphreys, "The price of anarchy in active signal landscape map building," in *Proceedings of IEEE Global Conference on Signal and Information Processing*, December 2013.

[21] C. Leung, S. Huang, and G. Dissanayake, "Active SLAM using model predictive control and attractor based exploration," in *Proceedings of IEEE/RSJ International Conference on Intelligent Robots and Systems*, October 2006, pp. 5026–5031.

[22] G. Lidoris, K. Kuhnlenz, D. Wollherr, and M. Buss, "Combined trajectory planning and gaze direction control for robotic exploration," in *Proceedings IEEE International Conference on Robotics and Automation*, April 2007, pp. 4044–4049.
[23] Z. Kassas, J. Bhatti, and T. Humphreys, "Receding horizon trajectory optimization for simultaneous signal landscape mapping and receiver localization," in *Proceedings of the ION GNSS*, September 2013.
[24] A. Thompson, J. Moran, and G. Swenson, *Interferometry and Synthesis in Radio Astronomy*, 2nd ed. John Wiley & Sons, 2001.
[25] Y. Bar-Shalom, X. Li, and T. Kirubarajan, *Estimation with Applications to Tracking and Navigation*, 1st ed. New York, NY: John Wiley & Sons, 2002.
[26] M. Psiaki and S. Mohiuddin, "Modeling, analysis, and simulation of GPS carrier phase for spacecraft relative navigation," *Journal of Guidance, Control, and Dynamics*, vol. 30, no. 6, pp. 1628–1639, November-December 2007.
[27] R. Hermann and A. Krener, "Nonlinear controllability and observability," *IEEE Transactions on Automatic Control*, vol. 22, no. 5, pp. 728–740, October 1977.
[28] M. Anguelova, "Observability and identifiability of nonlinear systems with applications in biology," Ph.D. dissertation, Chalmers University Of Technology and Göteborg University, Sweden, 2007.
[29] W. Respondek, "Geometry of static and dynamic feedback," in *Lecture Notes at the Summer School on Mathematical Control Theory*, Trieste, Italy, September 2001.
[30] J. Casti, "Recent developments and future perspectives in nonlinear system theory," *SIAM Review*, vol. 24, no. 3, pp. 301–331, July 1982.

PLACE PHOTO HERE

Zaher (Zak) M. Kassas (S'98-M'08-SM'011) is an assistant professor in the Department of Electrical Engineering at The University of California, Riverside. He received a B.E. with Honors in Electrical Engineering from The Lebanese American University, a M.S. in Electrical and Computer Engineering from The Ohio State University, and a M.S.E. in Aerospace Engineering and a Ph.D in Electrical and Computer Engineering from The University of Texas at Austin. From 2004 to 2010 he was a research and development engineer with the Control Design and Dynamical Systems Simulation Group at National Instruments Corp. His research interests include estimation, navigation, autonomous vehicles, control systems, and ITS.

PLACE PHOTO HERE

Todd E. Humphreys (M'12) is an assistant professor in the Department of Aerospace Engineering and Engineering Mechanics at The University of Texas at Austin and Director of The University of Texas Radionavigation Laboratory. He received a B.S. and M.S. in Electrical and Computer Engineering from Utah State University and a Ph.D. in Aerospace Engineering from Cornell University. His research interests are in estimation and filtering, GNSS technology, GNSS-based study of the ionosphere and neutral atmosphere, and GNSS security and integrity.